

See discussions, stats, and author profiles for this publication at: <https://www.researchgate.net/publication/230573798>

# Unexpected T-cell recognition of an altered peptide ligand is driven by reversed thermodynamics

ARTICLE *in* EUROPEAN JOURNAL OF IMMUNOLOGY · NOVEMBER 2012

Impact Factor: 4.03 · DOI: 10.1002/eji.201242588 · Source: PubMed

---

CITATIONS

5

READS

59

12 AUTHORS, INCLUDING:



[Chaithanya Madhurantakam](#)

TERI University

20 PUBLICATIONS 178 CITATIONS

[SEE PROFILE](#)



[Sebastian Grimm](#)

Molecular Partners

13 PUBLICATIONS 156 CITATIONS

[SEE PROFILE](#)



[Tatyana Sandalova](#)

Karolinska Institutet

65 PUBLICATIONS 1,272 CITATIONS

[SEE PROFILE](#)



[Adnane Achour](#)

Karolinska Institutet

86 PUBLICATIONS 1,282 CITATIONS

[SEE PROFILE](#)

# Unexpected T-cell recognition of an altered peptide ligand is driven by reversed thermodynamics

Eva B. Allerbring<sup>\*1</sup>, Adil D. Duru<sup>\*1</sup>, Hannes Uchtenhagen<sup>1</sup>, Chaithanya Madhurantakam<sup>1</sup>, Markus B. Tomek<sup>1</sup>, Sebastian Grimm<sup>2</sup>, Pooja A. Mazumdar<sup>1</sup>, Rosmarie Friemann<sup>3</sup>, Michael Uhlin<sup>4</sup>, Tatyana Sandalova<sup>1</sup>, Per-Åke Nygren<sup>\*\*2</sup> and Adnane Achour<sup>\*\*1</sup>

<sup>1</sup> Center for Infectious Medicine (CIM), Department of Medicine, Karolinska University Hospital Huddinge, Karolinska Institutet, Stockholm, Sweden

<sup>2</sup> Division of Molecular Biotechnology, School of Biotechnology, AlbaNova University Center, Royal Institute of Technology (KTH), Stockholm, Sweden

<sup>3</sup> Department of Chemistry, Biochemistry and Biophysics, University of Gothenburg, Gothenburg, Sweden

<sup>4</sup> Department of Microbiology, Tumor and Cell Biology (MTC), Karolinska Institutet, Stockholm, Sweden

The molecular basis underlying T-cell recognition of MHC molecules presenting altered peptide ligands is still not well-established. A hierarchy of T-cell activation by MHC class I-restricted altered peptide ligands has been defined using the T-cell receptor P14 specific for H-2D<sup>b</sup> in complex with the immunodominant lymphocytic choriomeningitis virus peptide gp33 (KAVYNFATM). While substitution of tyrosine to phenylalanine (Y4F) or serine (Y4S) abolished recognition by P14, the TCR unexpectedly recognized H-2D<sup>b</sup> in complex with the alanine-substituted semiagonist Y4A, which displayed the most significant structural modification. The observed functional hierarchy gp33 > Y4A > Y4S = Y4F was neither due to higher stabilization capacity nor to differences in structural conformation. However, thermodynamic analysis demonstrated that while recognition of the full agonist H-2D<sup>b</sup>/gp33 was strictly enthalpy driven, recognition of the weak agonist H-2D<sup>b</sup>/Y4A was instead entropy driven with a large reduction in the favorable enthalpy term. The fourfold larger negative heat capacity derived for the interaction of P14 with H-2D<sup>b</sup>/gp33 compared with H-2D<sup>b</sup>/Y4A can possibly be explained by higher water entrapment at the TCR/MHC interface, which is also consistent with the measured opposite entropy contributions for the interactions of P14 with both MHCs. In conclusion, this study demonstrates that P14 makes use of different strategies to adapt to structural modifications in the MHC/peptide complex.

**Keywords:** MHC · Molecular immunology · Protein–protein interactions · Structural biology · TCR



Supporting Information available online

## Introduction

Recognition of MHC molecules bound to peptides (pMHCs) by TCRs is a critical step for the initiation of T-cell responses.

Although this interaction is considered as highly specific, it is now well established that TCRs may also recognize other pMHCs [1–6]. The activation of T cells can be modulated by alterations in the presented peptides [7,8], the CDR loops of the TCR [9] and the

**Correspondence:** Dr. Adnane Achour  
e-mail: adnane.achour@ki.se

\*These authors contributed equally to this work.

\*\*These authors shared senior authorship.

$\alpha_1\alpha_2$ -domains of MHC molecules [10–13]. Depending on the quality of the triggered immune responses, APLs can be classified as: (i) agonists with the capacity to trigger a full range of T-cell activation events including TCR downregulation, cytokine production, granule release, and proliferation; (ii) weak agonists with the ability to induce lower magnitudes of TCR activation; (iii) partial agonists that may evoke a fraction of the events that characterize full T-cell activation; (iv) null peptides with no effect; or (v) antagonists that inhibit immune responses triggered by agonists.

The slowly increasing number of TCR/pMHC crystal structures has started to provide important insights into a few common structural properties. Most TCRs engage pMHCs in an approximately diagonal orientation [14] with weak to moderate-binding affinity [15]. It has been postulated that the CDR1 and CDR2 loops of the TCR mainly bind to MHC residues while the CDR3 loops mostly interact with the peptide, leading to the conclusion that TCR/pMHC antigen specificity is primarily governed by contacts between CDR3 loops and specific peptide residues. However, recent analysis of the current structural database of TCR/pMHC revealed that CDR1 loops also commonly contact the peptides [16–18]. Thus, although atomic understanding of the structural details of TCRs and pMHCs both alone and in complex has been acquired, the molecular basis underlying MHC recognition remains elusive and generally valid models for the modulation of TCR responses by APLs have still not been established. Indeed, we are still unable to predict both the binding affinity and the functional outcome of this interaction.

Three recent studies have provided important insights into the contribution of TCR/pMHC-binding kinetics to T-cell activation through 2D measurements using intact cells. These studies demonstrated that the on-rate rather than the off-rate correlated better with T-cell responsiveness when compared with 3D kinetics measured with surface plasmon resonance (SPR). Furthermore, the two-dimensional kinetics were faster, and the affinities of TCRs to pMHC complexes were clearly higher than previously estimated [19–21]. However, SPR has proven in most cases to be an excellent technique when comparing TCR affinities for different ligands, with a good correlation to functional studies [22–25]. While early thermodynamic experiments with SPR suggested that TCR/pMHC interactions were governed by enthalpically favorable and entropically unfavorable thermodynamics [4, 26–32], more

recent studies clearly demonstrated that recognition of pMHCs by TCRs could also be entropically driven [4, 5, 13, 15, 30, 33]. Thus at the present time, no clear-cut conclusions can be drawn regarding the strategy used by TCRs in order to recognize their cognate ligands.

Although the capacity of a TCR to recognize the same MHC in complex with a panel of APLs has been analyzed in several previous studies [2, 7, 32–36], the molecular basis underlying TCR recognition and discrimination of different pMHCs still remains poorly understood. In particular, the biochemical parameters, structural differences, and thermodynamic signatures used by TCRs to recognize MHC molecules presenting full or partial agonist peptides would be valuable to further assess the importance of key molecular parameters underlying T-cell activation [30, 33, 37, 38]. A hierarchical set of MHC-restricted peptides has previously been described for the TCR P14 specific for H-2D<sup>b</sup> in complex with the lymphocytic choriomeningitis virus-derived peptide gp33 (KAVYNFATM) [39–42] (Table 1). The immunodominant agonist gp33 induces complete CD8<sup>+</sup> T-cell activity including granule and calcium release, as well as cytokine production, proliferation, and cytotoxicity [40–42]. Crystal structures of H-2D<sup>b</sup>/gp33 revealed that the side chains of the tyrosine and phenylalanine peptide residues p4Y and p6F project out of the peptide-binding cleft, likely acting as main TCR contacts [43–46]. Upon CTL selection pressure, p4Y can be mutated to a phenylalanine (Y4F) [47] lowering the affinity of P14 to H-2D<sup>b</sup>/Y4F by a 100-fold [45] thereby abolishing T-cell mediated immune responses against the lymphocytic choriomeningitis virus infection [22, 42, 47]. Similarly, substitution of p4Y to a serine (Y4S) in the antagonist H-2D<sup>b</sup>/Y4S significantly reduced recognition by P14 [40]. In contrast, the weak/partial agonist H-2D<sup>b</sup>/Y4A in which p4Y was substituted to an alanine (Y4A) was still recognized by P14 [22, 41] although it carried the most significant structural alteration when compared with both Y4F and Y4S [48].

The present study aimed at further understanding how P14, with high specificity for H-2D<sup>b</sup>/gp33, is still able to recognize H-2D<sup>b</sup>/Y4A but neither H-2D<sup>b</sup>/Y4F nor H-2D<sup>b</sup>/Y4S. SPR analysis demonstrated that the binding affinity of P14 to each pMHC corresponded to the functional peptide hierarchy. The unexpected recognition of H-2D<sup>b</sup>/Y4A by P14 was not due to a higher stabilization capacity when compared with the other three pMHCs.

**Table 1.** Kinetic and thermodynamic parameters from P14 binding to H-2D<sup>b</sup> in complex with gp33, Y4A, Y4S, and Y4F at 25°C

Peptide	Sequence	K <sub>D</sub> ( $\mu$ M) <sup>a)</sup>	K <sub>d</sub> (s <sup>-1</sup> ) <sup>b)</sup>	K <sub>a</sub> (10 <sup>5</sup> /M·s) <sup>c)</sup>	TΔS (kcal/mol) <sup>e)</sup>	ΔH (kcal/mol) <sup>e)</sup>	ΔG (kcal/mol) <sup>d)</sup>	ΔCp (cal/mol·K)
gp33	KAVYNFATM	8.6 ± 0.4	0.5 ± 0.003	0.60	−9.0 ± 2.6	−15.8 ± 2.6	−6.9 ± 0.027	−755
Y4A	KAVANFATM	58.6 ± 4.2	0.7 ± 0.004	0.13	2.8 ± 1.4	−2.9 ± 1.3	−5.8 ± 0.044	−174
Y4S	KAVSNFATM	N.D.	N.D.	N.D.	−	−	N.D.	−
Y4F	KAVFNFATM	N.D.	N.D.	N.D.	−	−	N.D.	−

<sup>a)</sup> Determined from steady state SPR data with software BIAscan. The value is a mean ± SD of two independent experiments.

<sup>b)</sup> Determined from kinetic SPR data with software BIAscan. The value is a mean ± SD of two independent experiments.

<sup>c)</sup> Calculated from k<sub>d</sub>/K<sub>D</sub> = k<sub>a</sub>.

<sup>d)</sup> Calculated from ΔG = RT ln K<sub>D</sub>.

<sup>e)</sup> Calculated from fitting experimental values to a non-linear van't Hoff equation in GraphPad Prism 5. Mean ± SEM.

N.D. = Nondeterminable. Y4S and Y4F were not included in the thermodynamic study.

Furthermore, comparative crystal structure analysis of the pMHCs demonstrated similar conformations of the four peptides. However, thermodynamic SPR analysis demonstrated that P14 makes use of different strategies to adapt to the pMHCs. While recognition of the full agonist H-2D<sup>b</sup>/gp33 was strictly enthalpy driven, recognition of the weak agonist H-2D<sup>b</sup>/Y4A was instead entropy driven with a large reduction in the favorable enthalpy term.

## Results

### In contrast to H-2D<sup>b</sup>/Y4F and H-2D<sup>b</sup>/Y4S, H-2D<sup>b</sup>/Y4A is recognized by the H-2D<sup>b</sup>/gp33-specific TCR P14

This study was initiated with comparative analyses of TCR recognition of H-2D<sup>b</sup> in complex with gp33, Y4A, Y4S, or Y4F by P14 (Fig. 1). The magnitude of TCR internalization correlates with the

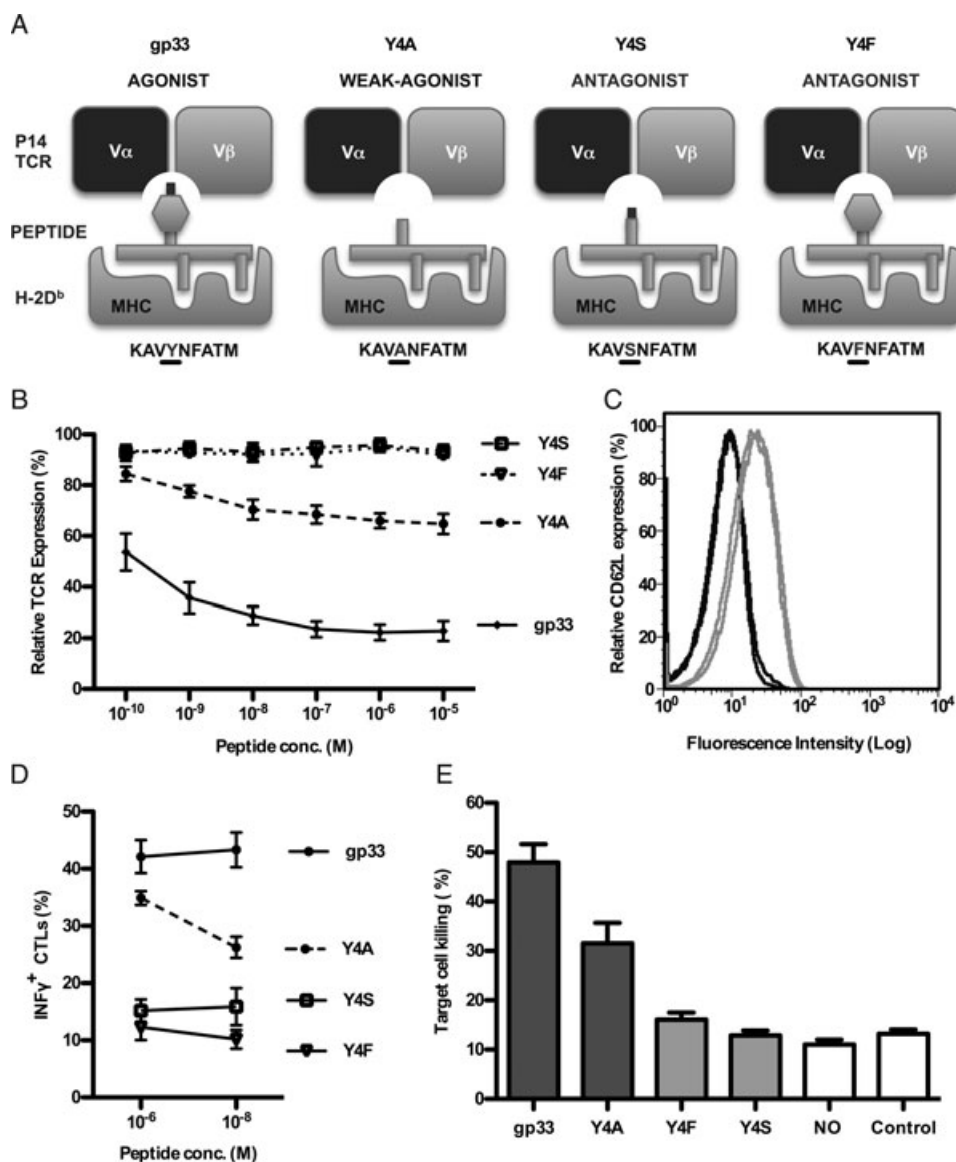


**Figure 1.** In contrast to H-2D<sup>b</sup>/Y4F and H-2D<sup>b</sup>/Y4S, H-2D<sup>b</sup>/Y4A is recognized by P14. (A) Schematic representation of P14 in complex with H-2D<sup>b</sup> presenting the four peptides. The sequence of each peptide is indicated below the schemes with the main peptide TCR-interacting position underlined. The side chains of the main peptide anchor residues at position 5 and 9 are represented by vertical sticks pointing down toward a schematic representation of the peptide-binding cleft of H-2D<sup>b</sup>. Phenyl rings are represented by hexagons while hydroxyl tips are colored in black. (B) P14 downregulation was estimated by staining RMA cells, pulsed with gp33, Y4A, Y4F, or Y4S, with anti-TCR Vα2 antibody. (C) CD62L expression levels in P14 T cells were measured following five hours stimulation with RMA cells pulsed with gp33, Y4A (black lines), Y4S, and Y4F (gray lines). One representative experiment out of three is displayed. (D) Intracellular IFN-γ expression levels were measured following five hours' stimulation with RMA cells pulsed with 10<sup>-6</sup> and 10<sup>-8</sup> M peptides. (E) Killing of RMA cells, pulsed with gp33, Y4A, Y4F, or Y4S, by P14 T cells was assessed in a 4 h chromium-release assay. Negative controls included the H-2D<sup>b</sup>-restricted influenza-derived peptide NP<sub>366</sub> (control) or no peptide (NO). Data in B, D, and E are shown as mean ± SEM from at least two pooled replicates from two independent experiments.

potency of TCR/pMHC interaction [40]. While exposure of P14 T cells to H-2D<sup>b</sup>/gp33 resulted in significant downregulation of P14, no TCR downregulation was detected with Y4S or Y4F. In contrast, Y4A induced intermediate downregulation of P14 (Fig. 1B). While both Y4S and Y4F failed to induce any proliferation, P14 CD8<sup>+</sup> T cells proliferated when exposed to gp33 or Y4A (data not included). In addition, decreased CD62L expression, also associated with T-cell activation, was observed in P14 T cells stimulated with gp33 or Y4A, but not when exposed to Y4S or Y4F (Fig. 1C). Furthermore, high and intermediate levels of intracellular IFN- $\gamma$  production were measured in P14 T cells stimulated with either gp33 or Y4A, respectively, whereas no IFN- $\gamma$  was produced upon stimulation with Y4S or Y4F (Fig. 1D). Finally, while P14 T-cell killing efficiency of gp33- and Y4A-pulsed cells was high and intermediate, respectively, Y4S- and Y4F-pulsed cells were not killed (Fig. 1E). In summary, our functional results clearly demonstrate that P14 T cells recognize H-2D<sup>b</sup>/gp33 and H-2D<sup>b</sup>/Y4A but not H-2D<sup>b</sup>/Y4S nor H-2D<sup>b</sup>/Y4F, reflecting a peptide hierarchy that can be described as gp33>Y4A>Y4S = Y4F.

### The unexpected recognition of H-2D<sup>b</sup>/Y4A by P14 is not due to a higher pMHC stabilization capacity

The four peptides display equivalent binding affinities to H-2D<sup>b</sup> and similar capacities to stabilize H-2D<sup>b</sup> cell surface expression levels on TAP-deficient cells (Supporting Information Fig. 1). Furthermore, the thermo-stability of soluble H-2D<sup>b</sup> in complex with each peptide was also investigated using circular dichroism (CD). The melting temperatures ( $T_m$ ), derived from changes in ellipticity at 218 nm, corresponding to loss of secondary structure during denaturation were similar for all four pMHCs (Fig. 2), with small variations that did not correspond to the functional peptide hierarchy. In conclusion, the differential activation of P14 T cells by the four pMHCs cannot be explained by differences in stabilization capacities.

### Differential thermodynamic recognition of H-2D<sup>b</sup>/gp33 and H-2D<sup>b</sup>/Y4A by the TCR P14

The binding affinities of P14 to the four pMHCs were measured using SPR (Supporting Information Fig. 2 and Table 1). The affinity of P14 to H-2D<sup>b</sup>/gp33, measured to 8.6  $\mu$ M, is within the range of previously reported values for this interaction [22, 23, 45, 49]. The affinity of P14 to H-2D<sup>b</sup>/Y4A was determined to 58.6  $\mu$ M. Conversely, it was not possible to determine an accurate  $K_D$ -value for the very weak interaction of P14 with H-2D<sup>b</sup>/Y4F. Finally, P14 did not bind to H-2D<sup>b</sup>/Y4S. In conclusion, the measured affinities for P14 to each pMHC reflect well the functional peptide hierarchy.

Kinetic-binding parameters were also calculated for the interaction of P14 with H-2D<sup>b</sup>/gp33 and H-2D<sup>b</sup>/Y4A. While the dissociation rates of P14 from both pMHCs can be considered as similar, the association rates derived from the equation  $k_a =$

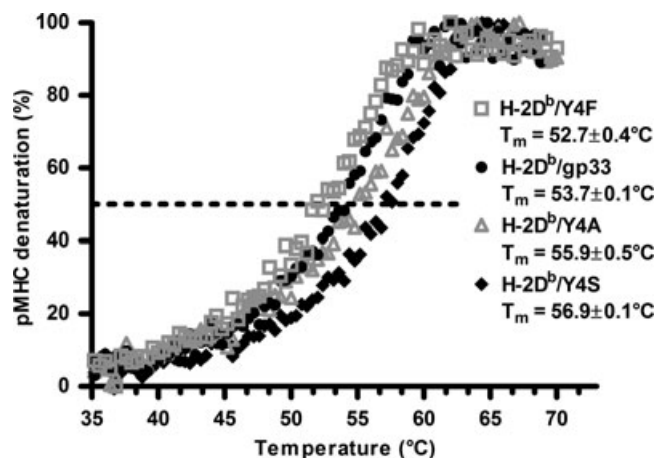


**Figure 2.** The four peptides display similar MHC stabilization capacity. Melting temperatures ( $T_m$ ), measured using CD, were derived from normalized thermal denaturation curves for H-2D<sup>b</sup>/gp33, H-2D<sup>b</sup>/Y4A, H-2D<sup>b</sup>/Y4S, and H-2D<sup>b</sup>/Y4F as the temperatures corresponding to 50% denaturation (dashed line). The indicated  $T_m$ -values are shown as averages  $\pm$  SD from at least three measurements with representative denaturation curves displayed. Data shown are representative of two pooled replicates from two independent experiments performed.

$k_d/K_D$  indicate a slower association rate of P14 with H-2D<sup>b</sup>/Y4A compared with that with H-2D<sup>b</sup>/gp33 (Table 1). The thermodynamic signatures characterizing the recognition of H-2D<sup>b</sup>/gp33 and H-2D<sup>b</sup>/Y4A by P14 were determined by affinity measurements over a temperature interval ranging from 5 to 30°C. Importantly, Helmholtz–Gibbs plots indicated that the profile of recognition used by P14 was different for the two pMHCs (Fig. 3A). While recognition of H-2D<sup>b</sup>/gp33 was enthalpy driven, recognition of H-2D<sup>b</sup>/Y4A was instead entropy driven with a large reduction in the favorable enthalpy term (Fig. 3B and Table 1). These results suggest that several intermolecular interactions are lost upon mutating position 4 of gp33 to alanine, accounting for the strongly reduced role of enthalpy in the binding of P14 to H-2D<sup>b</sup>/Y4A [13]. Furthermore, the heat capacities ( $\Delta C_p$ ) for both interactions were negative and within the range of what have previously been measured for pMHC-TCR interactions [15]. However, the binding of P14 to H-2D<sup>b</sup>/gp33 displayed a fourfold larger negative  $\Delta C_p$  value compared with the binding of P14 to H-2D<sup>b</sup>/Y4A (Table 1).

### The crystal structures of the four pMHC complexes are very similar

In an attempt to identify a possible structural basis for the differential recognition by P14, the crystal structures of H-2D<sup>b</sup>/Y4A and H-2D<sup>b</sup>/Y4S were determined to 2.4 and 2.0 Å resolution, respectively (Table 2), and compared with the previously determined crystal structures of H-2D<sup>b</sup>/gp33 [43, 44] and H-2D<sup>b</sup>/Y4F [48]. The overall structures of the four pMHCs were similar with root mean square deviations (rmsd) for the  $\alpha_1\alpha_2$  domains of H-2D<sup>b</sup>/gp33 with H-2D<sup>b</sup>/Y4A, H-2D<sup>b</sup>/Y4S, and H-2D<sup>b</sup>/Y4F of

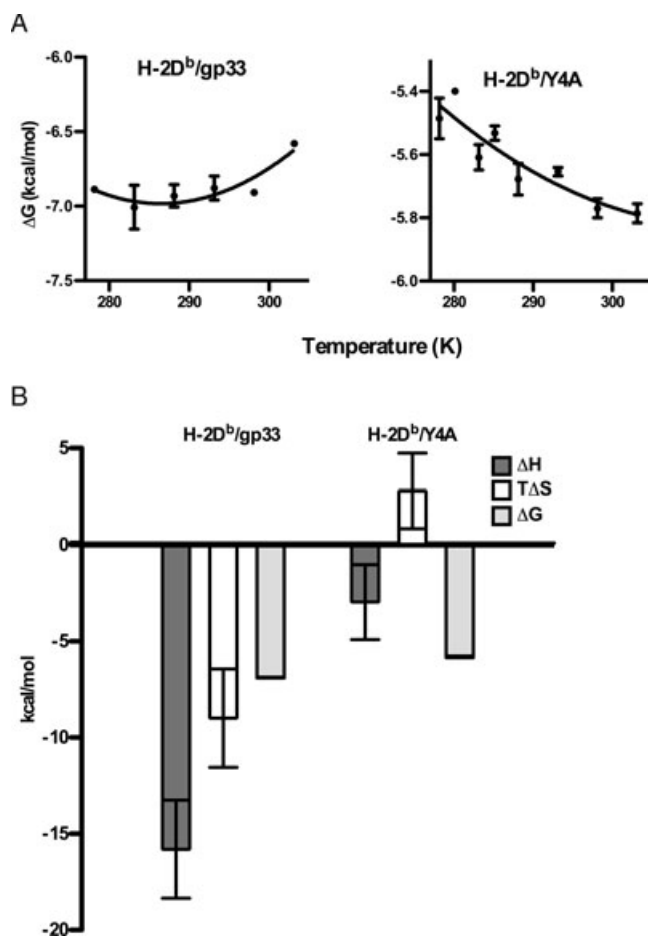


**Figure 3.** While recognition of H-2D<sup>b</sup>/gp33 is solely enthalpy driven, recognition of H-2D<sup>b</sup>/Y4A is both entropy and enthalpy driven. (A)  $K_D$  values were measured between 278 and 303 K. The overall binding energy,  $\Delta G$ , was derived from the equation  $\Delta G = RT\ln K_D$ . The thermodynamic parameters  $\Delta H$  and  $\Delta S$  were obtained from the nonlinear van't Hoff equation ( $\Delta G = \Delta H_{T_0} - T\Delta S_{T_0} + \Delta C_p(T-T_0) - T\Delta C_p \cdot \ln(T/T_0)$ , where  $T_0 = 298.15$  K). Each data point represents an average of at least two independent measurements  $\pm$  SEM. (B) Comparison of the thermodynamic parameters underlying interactions between P14 and H-2D<sup>b</sup>/gp33 (left) and H-2D<sup>b</sup>/Y4A (right). The energetic profiles are described by changes in free energy ( $\Delta G$ ), enthalpy ( $\Delta H$ ), and entropy ( $T\Delta S$ ). The bars represent mean  $\pm$  SEM of one replicate from two independent experiments.

0.33, 0.27, and 0.25 Å, respectively. The total amount of interactions formed between the four different peptides and H-2D<sup>b</sup> was also equivalent (Supporting Information Fig. 3).

Besides subtle differences in peptide residues p1K and p6F, the overall conformation of the four epitopes was remarkably similar (Fig. 4A), with rmsd values of 0.29, 0.26, and 0.22 Å when comparing gp33 with Y4A, Y4S, and Y4F, respectively. As for gp33 [43, 44] and Y4F [48], both Y4A and Y4S bind to H-2D<sup>b</sup> with residues p5N and p9M as main and p3V as secondary anchor positions. Similarly to p4Y, the side chains of p4F, p4S, and p4A protrude toward the TCR but, due to their decreasing sizes, are progressively embedded within the peptide-binding cleft of H-2D<sup>b</sup> (Fig. 1A and 4A). Removal of the aromatic ring at p4 results in a different conformation of the side chain of p6F in both H-2D<sup>b</sup>/Y4A and H-2D<sup>b</sup>/Y4S

**Table 2.** Data collection and refinement statistics<sup>a</sup>

Data collection	H-2D <sup>b</sup> /Y4A	H-2D <sup>b</sup> /Y4S
PDB ID	3QUK	3QUL
Wavelength (Å)	—	—
Space group	C2	P2 <sub>1</sub>
<i>a</i> (Å), <i>b</i> (Å), <i>c</i> (Å)	118.5, 126.2, 96.4	92.0, 122.7, 99.1
Beamline	—	—
Resolution (Å)	36.2–2.4 (2.5–2.4)	96.7–2.0 (2.1–2.0)
Number of observed reflections	—	—
Number of unique reflections	44615 (5419)	150031 (19978)
Redundancy	3.7 (3.5)	3.2 (3.7)
Completeness (%)	98.9 (81.0)	89.9 (56.3)
$R_{\text{merge}}^{\dagger}$ (%) <sup>b</sup>	5.2 (21.3)	8.2 (32.7)
$I/\sigma(I)$	20.0 (4.7)	13.2 (3.9)
Refinement statistics		
Resolution of data (Å)		
$R_{\text{cryst}}$ (%) <sup>c</sup>	24.2	20.7
$R_{\text{free}}$ (%) <sup>d</sup>	28.5	23.4
Number of protein atoms	6156	12609
Number of solvent atoms	301	915
Number of chains		
Rmsd from ideal geometry		
Bond length (Å)	0.009	0.009
Bond angles (°)	1.192	1.222
Ramachandran plot (%)		
Residues in preferred regions	94.4	96.7
Residues in allowed regions	5.3	2.8
Outliers	0.3	0.5
Wilson B-value (Å <sup>2</sup> )		
Average B-value (Å <sup>2</sup> )		
Protein	56.6	39.1
Solvent	54.8	44.4

<sup>a</sup>Values in parentheses are for the highest resolution shell.

<sup>b</sup> $R_{\text{merge}} = \sum_{hkl} \sum_i I_i(hkl) - \langle I(hkl) \rangle / \sum_{hkl} \sum_i I_i(hkl)$ , where  $I_i(hkl)$  is the *i*th observation of reflection  $hkl$  and  $\langle I(hkl) \rangle$  is the weighted average intensity for all observations *i* of reflection  $hkl$ .

<sup>c</sup> $R_{\text{cryst}} = \sum |F_o| - |F_c| / \sum |F_o|$ , where  $|F_o|$  and  $|F_c|$  are the observed and calculated structure factor amplitudes of a particular reflection and the summation is over 95% of the reflections in the specified resolution range. The remaining 5% of the reflections were randomly selected (test set) before the structure refinement and not included in the structure refinement.

<sup>d</sup> $R_{\text{free}}$  was calculated over these reflections using the same equation as for  $R_{\text{cryst}}$ .

compared with H-2D<sup>b</sup>/gp33 and H-2D<sup>b</sup>/Y4F. As a result, the conformation of the side chain of the neighboring MHC residue H155 is also altered (Fig. 4B). However, these observed structural differences cannot explain the discrepant functional potencies since they are shared by Y4A and Y4S. In contrast, the alternative conformation of the peptide lysine residue p1K is only present in Y4A (Fig. 4 and Supporting Information Fig. 3), and alters the

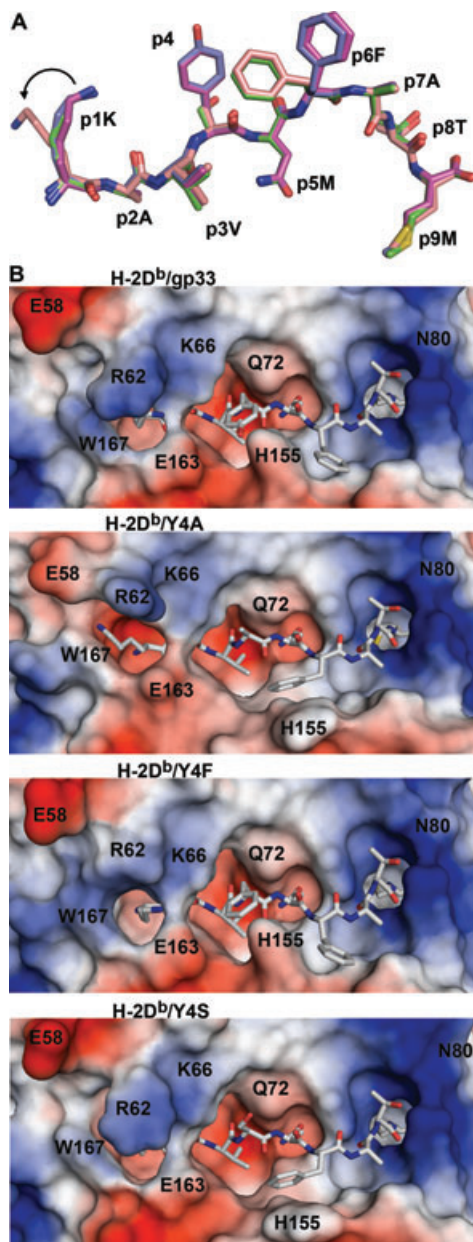


**Figure 4.** The conformation of the four peptides is nearly identical. (A) Superimposed side views of the four peptides gp33 (blue), Y4A (salmon), Y4S (green), and Y4F (magenta) following superposition of H-2D<sup>b</sup> residues 1–182. An arrow indicates conformational differences in the side chain of p1K. (B) The peptides, bound to H-2D<sup>b</sup>, are represented as sticks while the negatively and positively charged regions on the surface of H-2D<sup>b</sup> are indicated in red and blue, respectively. H-2D<sup>b</sup>-residues displaying significant conformational differences are indicated. Peptide residues are labeled with *p*.

conformation of the side chains of the adjacent  $\alpha_1$ -helix residues E58 and R62 that move closer together in H-2D<sup>b</sup>/Y4A (Fig. 4B).

Indeed, the importance of peptide position 1 for recognition by P14 has been previously demonstrated [46]. In the present study, substitution of p1K to serine in Y4A and gp33 abrogated in both cases P14 downregulation and recognition of (K1S, Y4A) and of K1S (Fig. 5). Similarly, mutation of p1K to leucine in Y4A

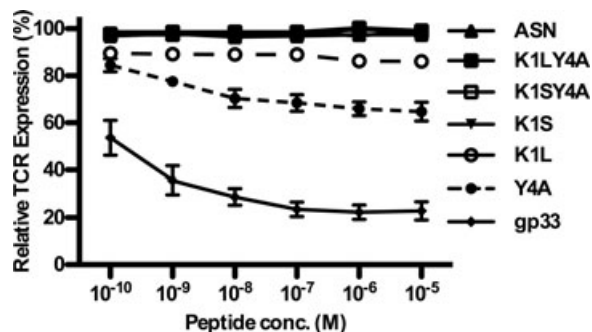


**Figure 5.** Recognition of the semiagonist Y4A by P14 is abrogated upon mutation of p1K to serine or leucine. TCR downregulation was assessed following exposure of P14 T cells to RMA cells, prepulsed with different concentrations of peptides gp33, Y4A, gp33(K1L), gp33(K1S,Y4A) gp33(K1L,Y4A), gp33(K1S), and the control peptide NP<sub>366</sub>. The presented results are an average of two independent experiments  $\pm$  SEM.

abolished P14 downregulation while the capacity of K1L to downregulate P14 expression levels was strongly reduced (Fig. 5). Additionally, previous affinity measurements using SPR demonstrated that methionine (p1M), arginine (p1R), and serine (p1S) substitutions all significantly reduced P14 affinity to H-2D<sup>b</sup>/gp33 [22]. In conclusion, our results indicate that p1K is crucial for recognition of both H-2D<sup>b</sup>/gp33 and H-2D<sup>b</sup>/Y4A by P14. However, our structural analysis does not provide clear-cut evidence underlying how the same TCR may adapt to these two different pMHCs. Only the determination of the ternary TCR/pMHC crystal structures will provide an exact understanding of the recognition of these two pMHC molecules by P14.

The role of water molecules is important in both protein folding and protein–protein interactions. Since favorable entropy changes in protein–protein interactions commonly arise from desolvation (i.e. the hydrophobic effect), we further compared the four crystal structures for differences in water disposition within the TCR-binding interface of the pMHCs. It should however be noted that since the four pMHCs crystallized in different space groups with different resolutions, our analysis of water contents should be considered as speculative. While similar amounts of water molecules were found in the TCR-binding interfaces of the four pMHC molecules, our analysis also suggested that waters were more coordinated to H-2D<sup>b</sup>/Y4S, forming a network of hydrogen bonds with pMHC residues and/or other waters, especially around peptide position 4 (Supporting Information Fig. 4).

## Discussion

The molecular basis for TCR discrimination of MHC-restricted APLs is still not well understood. While some TCRs bind to MHC molecules in complex with wild-type peptides and APLs using different thermodynamic signatures [30, 38] other TCRs recognize different pMHCs using similar thermodynamic signatures [5, 25]. The present study focused on how modifications at the main peptide TCR-contact position could alter TCR recognition. In particular, we addressed how the H-2D<sup>b</sup>/gp33-specific TCR P14 can still

recognize H-2D<sup>b</sup>/Y4A that displays the largest structural modification, but not H-2D<sup>b</sup>/Y4F and H-2D<sup>b</sup>/Y4S, both with more conservative modifications.

Functional analysis of the capacity of gp33 and APLs to elicit P14 T-cell responses demonstrated a T-cell activation hierarchy that can be described as gp33 > Y4A > Y4S = Y4F (Fig. 1). It has previously been demonstrated that the capacity of MHC-restricted epitopes to elicit TCR responses is directly linked to their ability to stabilize these complexes [50–52]. However, the stabilization capacity of the four gp33-variants, tested using both cellular assays and CD measurements, demonstrated that the observed discrepant functional outcomes could not be explained by differences in peptide stabilization capacity (Fig. 2 and Supporting Information Fig. 1).

The binding affinity of P14 to each pMHC was measured using SPR (Supporting Information Fig. 2 and Table 1). The  $K_D$ -values of P14 for H-2D<sup>b</sup>/Y4F or H-2D<sup>b</sup>/Y4S were too low to be adequately determined with the concentrations used in this study. Conversely, we were able to determine the  $K_D$ -values for P14 interaction with H-2D<sup>b</sup>/gp33 and H-2D<sup>b</sup>/Y4A to 8.6  $\mu$ M and 58.6  $\mu$ M, respectively, demonstrating that the affinity of P14 to each pMHC corresponded to the observed functional hierarchy (Fig. 1). These values are consistent with the sixfold higher affinity previously reported for the interaction of P14 with H-2D<sup>b</sup>/gp33 compared with H-2D<sup>b</sup>/Y4A [45]. In general, a good correlation has been reported between affinities for TCR/pMHC interactions and functional T-cell responses. However, some exceptions to this rule have also been observed [19, 53, 54]. A possible explanation for the lack of correlation has been provided in a recent study that coupled T-cell antagonism to an unusual docking geometry of the TCR onto the pMHC [19].

Although structural analysis of the four pMHCs revealed that the conformations of the peptides were remarkably similar, few subtle differences were observed. In particular, the side chains of p1K as well as of E58 and R62 are different in H-2D<sup>b</sup>/Y4A when compared with those of the other three pMHCs (Fig. 4 and Supporting Information Fig. 3). It is noteworthy that the conformation of p1K in H-2D<sup>b</sup>/gp33(F6L), another semi-agonist, is similar to H-2D<sup>b</sup>/Y4A [48]. Furthermore, substitution of p1K to serine or leucine in both H-2D<sup>b</sup>/gp33 and H-2D<sup>b</sup>/Y4A abrogated or strongly reduced T-cell recognition (Fig. 5), indicating the importance of this peptide position for recognition by P14. It should also be noted that substitution of p1K in gp33 to serine in previous studies reduced the affinity of P14 by 30-fold [22, 46]. Indeed, the region comprising and surrounding p1K in H-2D<sup>b</sup> has been previously suggested as a secondary hotspot for TCR recognition [46]. To date the importance of the first peptide position for TCR recognition has been established for several MHC alleles including H-2D<sup>b</sup> [46], HLA-A2 [55], H-2K<sup>b</sup> [56] and HLA-B27 [46, 55, 57]. Thus, the results of our study further support the notion that peptide position 1 and surrounding MHC residues are crucial for P14 recognition.

In this study, we have demonstrated that P14 makes use of different thermodynamic signatures when binding the agonist H-2D<sup>b</sup>/gp33 compared with the weak agonist H-2D<sup>b</sup>/Y4A. While

recognition of H-2D<sup>b</sup>/gp33 was strictly enthalpy driven, recognition of H-2D<sup>b</sup>/Y4A was characterized by favorable entropy with a large reduction in the favorable enthalpy term (Fig. 3). The resulting change in enthalpy in a protein–protein interaction can be described as the sum of favorable enthalpy, derived from all inter- and intramolecular interactions formed, and unfavorable enthalpy that results from for example the displacement of water molecules from the binding interface [35]. The favorable  $\Delta H$  for the P14/H-2D<sup>b</sup>/gp33 interaction is most probably due to the formation of several intermolecular contacts. Conversely, the drastic reduction in favorable  $\Delta H$  for the P14/H-2D<sup>b</sup>/Y4A interaction could be explained by fewer intermolecular contacts following the mutation of tyrosine to alanine at p4 of gp33 [13]. However, interactions formed between CDR(s) of the TCR and MHC regions such as around p1K in H-2D<sup>b</sup>/Y4A may partially compensate for the loss of interactions between P14 and the region around p4A. Indeed, it has been previously demonstrated that TCRs may adapt to certain pMHCs through distinct conformations of the CDR3 loops that have an inherent flexibility, resulting in TCR cross-recognition [5, 58–60].

The role of water molecules is important in both protein folding and protein–protein interactions. Favorable entropy changes commonly arise from desolvation, whereby ordered waters are expelled from apolar surfaces upon binding, leading to an increase in total entropy of the system [35]. The release of water molecules upon binding of a TCR to a pMHC can thus result in a favorable entropy pathway for recognition, as clearly demonstrated in a previous study [29]. In contrast, poor shape complementary between TCRs and pMHC interfaces may result in formation of cavities that can trap waters, as observed in several TCR/pMHC crystal structures [29, 34]. Trapped water molecules can form hydrogen bonds, thus contributing positively to the binding enthalpy in TCR interactions. The binding interfaces of H-2D<sup>b</sup>/gp33 and H-2D<sup>b</sup>/Y4A appeared to contain an equivalent amount of water molecules with a similar degree of coordination (Supporting Information Fig. 4). The unfavorable entropy measured for P14/H-2D<sup>b</sup>/gp33 likely reflects an inherent loss of flexibility consistent with ordering of CDR loops and pMHC residues upon binding [9]. Conversely, the favorable entropy for recognition of H-2D<sup>b</sup>/Y4A by P14 could be a result of the possible increase in desolvation entropy in combination with a reduction of entropic cost upon ordering CDR loops well in line with the reduced  $\Delta H$  for this interaction.

A negative heat capacity is consistent with burial of hydrophobic surfaces [15] as well as entrapment of waters [61] and has also been connected to T-cell activation [30]. The  $\Delta C_p$ -values for the interactions of P14 with H-2D<sup>b</sup>/gp33 and H-2D<sup>b</sup>/Y4A were both negative and within the range of what have previously been measured for pMHC-TCR interactions [15]. However, binding of P14 to H-2D<sup>b</sup>/gp33 displayed a four times more negative  $\Delta C_p$ -value compared with binding to H-2D<sup>b</sup>/Y4A (Table 1). The less negative  $\Delta C_p$ -value for the interaction of P14 with H-2D<sup>b</sup>/Y4A could possibly be related to increased water displacement upon binding, in agreement with the measured favorable entropy for this interaction.

Although it remains puzzling to us why P14 does not recognize H-2D<sup>b</sup>/Y4S, several factors may provide a hypothetical explanation. Waters bound to H-2D<sup>b</sup>/Y4S seemed to be more coordinated, especially around the hydroxyl tip of p4S (Supporting Information Fig. 4). Indeed, peptide substitutions can be disruptive by means of reducing the overall ability to exclude waters from the interface [62]. We therefore speculate that tighter water coordination may lead to a higher enthalpic price for their displacement from the interface of H-2D<sup>b</sup>/Y4S. Furthermore, a suboptimal distance between the hydroxyl group of p4S and P14 could impair the formation of hydrogen bonds.

In conclusion, while it has been previously demonstrated that two different TCRs may recognize the same pMHC using different thermodynamic strategies [61], the present study clearly demonstrates that the same TCR may also respond to both the agonist H-2D<sup>b</sup>/gp33 and the semi-agonist H-2D<sup>b</sup>/Y4A through the use of different thermodynamic strategies.

## Materials and methods

### Cell lines and mice

TAP-deficient T2/H-2D<sup>b</sup> (T2-D<sup>b</sup>) cells, a kind gift from Prof. M.B.A. Oldstone (Scripps La Jolla, USA), were used in both peptide affinity and stabilization assays. H-2D<sup>b</sup> and H-2K<sup>b</sup>-positive RMA cells were used as target cells in TCR downregulation, chromium release, and intracellular INF- $\gamma$  production assays. Pathogen-free RAG1/2-deficient (RAG1/2<sup>-/-</sup>) and RAG1/2<sup>-/-</sup> P14-transgenic mice were bred and maintained within the animal facilities at the Department of Microbiology, Tumor and Cell Biology (MTC, Karolinska Institute). V $\alpha$ 2<sup>+</sup> T cells from P14-transgenic mice were used as effector cells in in vitro experiments. All procedures were performed with the appropriate ethical permit (N413/09) under Swedish national guidelines.

### Peptides and antibodies

Peptides gp33, Y4A, Y4S, Y4F as well as control peptides NP<sub>366</sub> (ASNEMETM) and P18-I10 (RGPGRAFVTI) were purchased from GenScript (Piscataway, NJ, USA). The antibodies KH95 (anti-H-2D<sup>b</sup>), 53–6.7 (anti-CD8 $\alpha$ ), MEL-14 (anti-CD62L), XMG1.2 (anti-INF- $\gamma$ ) and B20.1 (anti-TCR V $\alpha$ 2) were purchased from BD Biosciences (San Diego, CA, USA).

### TCR downregulation assays

P14-splenocytes were mixed with peptide-pulsed RMA cells at an effector:target (E:T) ratio of 10:1. Cells were coincubated at 37°C for 4 h, and stained with anti-CD8 $\alpha$  and anti-TCR V $\alpha$ 2. Flow cytometry was performed on a BD FACS Calibur and changes in MFI of the V $\alpha$ 2 staining used to estimate TCR downregulation.

## In vivo stimulation of P14 T cells and chromium release cytotoxicity assays

P14 TCR-transgenic mice were subcutaneously injected with 100 µg of gp33 in PBS or PBS only. Spleens were harvested six days later. Target RMA cells, labeled with Cr<sup>51</sup>, were pulsed with the indicated concentrations of peptides for one hour at 37°C and then mixed with in vivo stimulated P14 splenocytes at 10:1 E:T ratio followed by a standard four hours Cr<sup>51</sup>-release assay. Radioactivity was measured on a gamma-counter (Wallac, Uppsala, Sweden). The percentage of specific lysis was calculated as (Cr<sup>51</sup> release in test well-spontaneous Cr<sup>51</sup> release) / (maximum Cr<sup>51</sup> release-spontaneous Cr<sup>51</sup> release) × 100.

### INF- $\gamma$ production and CD62L expression

CD8 $^{+}$  T cells were isolated from spleens of in vivo stimulated P14-transgenic mice and cocultured with 10<sup>-6</sup> M peptide-pulsed RMA cells for 5 h. GolgiStop (BD Biosciences) was added after one hour of coincubation. Four hours later, washed cells were stained with anti-CD8 $\alpha$  and anti-CD62L antibodies, followed by permeabilization with the cytofix/cytoperm kit (BD Biosciences) and staining for intracellular INF- $\gamma$  expression with XMG1.2. Flow cytometry data sampling was performed on a CyAn instrument (Dako, Glostrup, Denmark) and analyzed with FlowJo software.

### Production and isolation of soluble TCR P14

Expression vectors encoding for the  $\alpha$ - and  $\beta$ -chains of P14 were kindly provided by Prof. Awen Gallimore (School of Medicine, Cardiff, UK). P14 was produced and refolded by dilution essentially as previously described [49]. Purification was performed using ion exchange followed by size exclusion chromatography. P14 was thereafter concentrated to 20 µg/mL.

### Preparation, refolding, and crystallization of H-2D<sup>b</sup>/Y4A and H-2D<sup>b</sup>/Y4S

pMHC refolding was conducted as previously described [63–65]. The best diffracting crystals for H-2D<sup>b</sup>/Y4A and H-2D<sup>b</sup>/Y4S were obtained by hanging drop vapor diffusion method in 1.8 M ammonium sulfate, 0.1 M Tris HCl pH 9.0. Typically, 4 µL of a 5 mg/mL protein solution in 20 mM Tris HCl pH 7.0 were mixed in a 4:2 ratio with the crystallization reservoir solution at 20°C.

### Data collection and processing

Data collection was performed under cryogenic conditions (T = 100 K) using a MAR CCD detector at beamline I711 at MaxLab (Lund, Sweden). Crystals were soaked during a short time in a cryoprotectant solution containing crystallization solution supplemented with 30% glycerol before freezing in liquid nitrogen. The

diffraction data were processed and scaled using the programs MOSFLM 7.0.3 [66] and SCALA [67] as implemented in CCP4. H-2D<sup>b</sup>/Y4S and diffracted H-2D<sup>b</sup>/Y4A diffracted at a resolution of 2.0 Å and 2.4 Å, respectively.

### Structure determination and refinement

The crystal structures of H-2D<sup>b</sup>/Y4A and H-2D<sup>b</sup>/Y4S were determined by molecular replacement using PHASER [68]. The crystal structure of H-2D<sup>b</sup>/gp33 (PDB ID: 1S7U) [48], with the peptide omitted, was used as a search model. Random 5% of the reflections were set aside for use as a test set for monitoring the refinement by  $R_{\text{free}}$  cross-validation. Refinement of the models was performed using Refmac5 [69] combined with model building using the program Coot [70]. Individual atom B-factors were refined isotropically. The position of all water molecules was inspected manually using Coot. The stereochemistry of the final models was verified using PROCHECK.

### Surface Plasmon Resonance-binding affinity and thermodynamic analyses

All measurements were performed on BIACore 2000 (GE Healthcare, USA) at 25 °C, essentially as previously described [49]. Soluble P14 was noncovalently coupled to the anti-C<sub>β</sub> antibody H57–597 (eBioscience Inc., USA). 8000 RUs of H57–597 were coupled to a CM5-chip, resulting in 3000 RUs of immobilized P14. A control surface without antibody was used as reference flow cell. Concentration series of pMHCs were injected over the chip. A flow rate of 10 µL/min was used for affinity measurements. A flow rate of 40 µL/min was used to verify the dissociation rates. These data were analyzed with BIAscan 2000 (BIACore AB, Uppsala, Sweden). The  $K_D$ -values were obtained from steady-state fitting of equilibrium-binding curves using GraphPad Prism 5 (GraphPad Software, La Jolla, USA). The reported  $K_D$ -values are an average of at least two independent measurements ± SD.

For the thermodynamic analyses  $K_D$ -values were measured from 5 to 30 °C in 2–5 °C increments.  $\Delta G$  was derived from the measured  $K_D$ -value using the equation  $\Delta G = RT \ln K_D$ .  $\Delta H$ ,  $\Delta S$ , and  $\Delta C_p$  were obtained by fitting the data to a nonlinear Van't Hoff equation ( $\Delta G = \Delta H_{T_0} \cdot T \Delta S_{T_0} + \Delta C_p(T-T_0) - T \Delta C_p \cdot \ln(T/T_0)$ , where  $T_0 = 298.15$  K). The reported  $K_D$ -value at each temperature point is an average of at least two independent experiments ± SEM.

### Analysis of pMHC stability using circular dichroism

CD measurements were performed in 20 mM K<sub>2</sub>HPO<sub>4</sub>/KH<sub>2</sub>PO<sub>4</sub> (pH 7.5) using protein concentrations from 0.15–0.25 mg/mL. Spectra were recorded with a JASCO J-810 spectropolarimeter (JASCO Analytical Instruments, Great Dunmow, UK) equipped with a thermoelectric temperature controller in a 2 mm cell. pMHC

denaturation was measured between 30–70 °C at 218 nm with a gradient of 48 °C/h at 0.1 °C increments and an averaging time of 8 s. The melting curves were scaled from 0–100% and the  $T_m$ -values extracted as the temperature at 50% denaturation. Curves and  $T_m$ -values are an average of at least three measurements from at least two independent refolding assays/complex. Spectra were analyzed using GraphPad Prism 5.

**Acknowledgments:** We gratefully acknowledge access to synchrotron beamlines 14.2 at ESRF (Grenoble, France), MX-41 at BESSY (Berlin, Germany) and I711 at MaxLab (Lund, Sweden). This work was supported by grants from the Swedish Research Council, the Swedish Cancer Society, the Swedish Childhood Cancer Foundation and the Swedish National Board of Health (AA).

**Conflict of interest:** The authors declare no financial or commercial conflict of interest.

### References

- Godfrey, D. I., Rossjohn, J. and McCluskey, J., The fidelity, occasional promiscuity, and versatility of T cell receptor recognition. *Immunity* 2008. 28: 304–314.
- Martinez-Hackert, E., Anikeeva, N., Kalams, S. A., Walker, B. D., Hendrickson, W. A. and Sykulev, Y., Structural basis for degenerate recognition of natural HIV peptide variants by cytotoxic lymphocytes. *J. Biol. Chem.* 2006. 281: 20205–20212.
- Borbulevych, O. Y., Santhanagopalan, S. M., Hossain, M. and Baker, B. M., TCRs used in cancer gene therapy cross-react with MART-1/Melan-A tumor antigens via distinct mechanisms. *J. Immunol.* 2011. 187: 2453–2463.
- Colf, L. A., Bankovich, A. J., Hanick, N. A., Bowerman, N. A., Jones, L. L., Kranz, D. M. and Garcia, K. C., How a single T cell receptor recognizes both self and foreign MHC. *Cell* 2007. 129: 135–146.
- Mazza, G., Auphan-Anezin, N., Gregoire, C., Guimezanes, A., Kellenberger, C., Roussel, A., Kearney, A. et al., How much can a T-cell antigen receptor adapt to structurally distinct antigenic peptides? *EMBO J.* 2007. 26: 1972–1983.
- Macdonald, W. A., Chen, Z., Gras, S., Archbold, J. K., Tynan, F. E., Clements, C. S., Bharadwaj, M. et al., T cell allorecognition via molecular mimicry. *Immunity* 2009. 31: 897–908.
- Baker, B. M., Gagnon, S. J., Biddison, W. E. and Wiley, D. C., Conversion of a T cell antagonist into an agonist by repairing a defect in the TCR/peptide/MHC interface: implications for TCR signaling. *Immunity* 2000. 13: 475–484.
- Sloan-Lancaster, J. and Allen, P. M., Altered peptide ligand-induced partial T cell activation: molecular mechanisms and role in T cell biology. *Annu. Rev. Immunol.* 1996. 14: 1–27.
- Jones, L. L., Colf, L. A., Bankovich, A. J., Stone, J. D., Gao, Y. G., Chan, C. M., Huang, R. H. et al., Different thermodynamic binding mechanisms and peptide fine specificities associated with a panel of structurally similar high-affinity T cell receptors. *Biochemistry* 2008. 47: 12398–12408.
- Baker, B. M., Turner, R. V., Gagnon, S. J., Wiley, D. C. and Biddison, W. E., Identification of a crucial energetic footprint on the alpha1 helix

- of human histocompatibility leukocyte antigen (HLA)-A2 that provides functional interactions for recognition by tax peptide/HLA-A2-specific T cell receptors. *J. Exp. Med.* 2001; **193**: 551–562.
- 11 Baxter, T. K., Gagnon, S. J., Davis-Harrison, R. L., Beck, J. C., Binz, A. K., Turner, R. V., Biddison, W. E. et al., Strategic mutations in the class I major histocompatibility complex HLA-A2 independently affect both peptide binding and T cell receptor recognition. *J. Biol. Chem.* 2004; **279**: 29175–29184.
  - 12 Gagnon, S. J., Borbulevych, O. Y., Davis-Harrison, R. L., Baxter, T. K., Clemens, J. R., Armstrong, K. M., Turner, R. V. et al., Unraveling a hotspot for TCR recognition on HLA-A2: evidence against the existence of peptide-independent TCR binding determinants. *J. Mol. Biol.* 2005; **353**: 556–573.
  - 13 Miller, P. J., Pazy, Y., Conti, B., Riddle, D., Appella, E. and Collins, E. J., Single MHC mutation eliminates enthalpy associated with T cell receptor binding. *J. Mol. Biol.* 2007; **373**: 315–327.
  - 14 Rudolph, M. G., Stanfield, R. L. and Wilson, I. A., How TCRs bind MHCs, peptides, and coreceptors. *Annu. Rev. Immunol.* 2006; **24**: 419–466.
  - 15 Armstrong, K. M., Insaidoo, F. K. and Baker, B. M., Thermodynamics of T-cell receptor-peptide/MHC interactions: progress and opportunities. *J. Mol. Recognit.* 2008; **21**: 275–287.
  - 16 Burrows, S. R., Chen, Z., Archbold, J. K., Tynan, F. E., Beddoe, T., Kjær Nielsen, L., Miles, J. J. et al., Hard wiring of T cell receptor specificity for the major histocompatibility complex is underpinned by TCR adaptability. *Proc. Natl. Acad. Sci. USA* 2010; **107**: 10608–10613.
  - 17 Cole, D. K., Yuan, F., Rizkallah, P. J., Miles, J. J., Gostick, E., Price, D. A., Gao, G. F. et al., Germ line-governed recognition of a cancer epitope by an immunodominant human T-cell receptor. *J. Biol. Chem.* 2009; **284**: 27281–27289.
  - 18 Gras, S., Chen, Z., Miles, J. J., Liu, Y. C., Bell, M. J., Sullivan, L. C., Kjær Nielsen, L. et al., Allelic polymorphism in the T cell receptor and its impact on immune responses. *J. Exp. Med.* 2010; **207**: 1555–1567.
  - 19 Adams, J. J., Narayanan, S., Liu, B., Birnbaum, M. E., Kruse, A. C., Bowerman, N. A., Chen, W. et al., T cell receptor signaling is limited by docking geometry to peptide-major histocompatibility complex. *Immunity* 2011; **35**: 681–693.
  - 20 Huang, J., Zarnitsyna, V. I., Liu, B., Edwards, L. J., Jiang, N., Evavold, B. D. and Zhu, C., The kinetics of two-dimensional TCR and pMHC interactions determine T-cell responsiveness. *Nature* 2004; **432**: 932–936.
  - 21 Huppa, J. B., Axmann, M., Mortelmaier, M. A., Lillemeier, B. F., Newell, E. W., Brameshuber, M., Klein, L. O. et al., TCR-peptide-MHC interactions in situ show accelerated kinetics and increased affinity. *Nature* 2003; **463**: 963–967.
  - 22 Tian, S., Maile, R., Collins, E. J. and Frelinger, J. A., CD8+ T cell activation is governed by TCR-peptide/MHC affinity, not dissociation rate. *J. Immunol.* 2007; **179**: 2952–2960.
  - 23 Boulter, J. M., Schmitz, N., Sewell, A. K., Godkin, A. J., Bachmann, M. F. and Gallimore, A. M., Potent T cell agonism mediated by a very rapid TCR/pMHC interaction. *Eur. J. Immunol.* 2007; **37**: 798–806.
  - 24 Chervin, A. S., Stone, J. D., Holler, P. D., Bai, A., Chen, J., Eisen, H. N. and Kranz, D. M., The impact of TCR-binding properties and antigen presentation format on T cell responsiveness. *J. Immunol.* 2009; **183**: 1166–1178.
  - 25 Aleksic, M., Dushek, O., Zhang, H., Shenderov, E., Chen, J. L., Cerundolo, V., Coombs, D. et al., Dependence of T cell antigen recognition on T cell receptor-peptide MHC confinement time. *Immunity* 2010; **32**: 163–174.
  - 26 Armstrong, K. M., Piepenbrink, K. H. and Baker, B. M., Conformational changes and flexibility in T-cell receptor recognition of peptide-MHC complexes. *Biochem. J.* 2008; **415**: 183–196.
  - 27 Boniface, J. J., Reich, Z., Lyons, D. S. and Davis, M. M., Thermodynamics of T cell receptor binding to peptide-MHC: evidence for a general mechanism of molecular scanning. *Proc. Natl. Acad. Sci. USA* 1999; **96**: 11446–11451.
  - 28 Davis-Harrison, R. L., Armstrong, K. M. and Baker, B. M., Two different T cell receptors use different thermodynamic strategies to recognize the same peptide/MHC ligand. *J. Mol. Biol.* 2005; **346**: 533–550.
  - 29 Ely, L. K., Beddoe, T., Clements, C. S., Matthews, J. M., Purcell, A. W., Kjær Nielsen, L., McCluskey, J. et al., Disparate thermodynamics governing T cell receptor-MHC-I interactions implicate extrinsic factors in guiding MHC restriction. *Proc. Natl. Acad. Sci. USA* 2006; **103**: 6641–6646.
  - 30 Krosgaard, M., Prado, N., Adams, E. J., He, X. L., Chow, D. C., Wilson, D. B., Garcia, K. C. et al., Evidence that structural rearrangements and/or flexibility during TCR binding can contribute to T cell activation. *Mol. Cell* 2003; **12**: 1367–1378.
  - 31 Lee, J. K., Stewart-Jones, G., Dong, T., Harlos, K., Di Gleria, K., Dorrell, L., Douek, D. C. et al., T cell cross-reactivity and conformational changes during TCR engagement. *J. Exp. Med.* 2004; **200**: 1455–1466.
  - 32 Willcox, B. E., Gao, G. F., Wyer, J. R., Ladbury, J. E., Bell, J. I., Jakobsen, B. K. and van der Merwe, P. A., TCR binding to peptide-MHC stabilizes a flexible recognition interface. *Immunity* 1999; **10**: 357–365.
  - 33 Persaud, S. P., Donermeyer, D. L., Weber, K. S., Kranz, D. M. and Allen, P. M., High-affinity T cell receptor differentiates cognate peptide-MHC and altered peptide ligands with distinct kinetics and thermodynamics. *Mol. Immunol.* 2007; **47**: 1793–1801.
  - 34 Ding, Y. H., Smith, K. J., Garboczi, D. N., Utz, U., Biddison, W. E. and Wiley, D. C., Two human T cell receptors bind in a similar diagonal mode to the HLA-A2/Tax peptide complex using different TCR amino acids. *Immunity* 1998; **8**: 403–411.
  - 35 Dressel, A., Chin, J. L., Sette, A., Gausling, R., Hollsberg, P. and Hafler, D. A., Autoantigen recognition by human CD8 T cell clones: enhanced agonist response induced by altered peptide ligands. *J. Immunol.* 1997; **159**: 4943–4951.
  - 36 Goldrath, A. W. and Bevan, M. J., Low-affinity ligands for the TCR drive proliferation of mature CD8+ T cells in lymphopenic hosts. *Immunity* 1999; **11**: 183–190.
  - 37 Borbulevych, O. Y., Piepenbrink, K. H., Gloor, B. E., Scott, D. R., Sommese, R. F., Cole, D. K., Sewell, A. K. et al., T cell receptor cross-reactivity directed by antigen-dependent tuning of peptide-MHC molecular flexibility. *Immunity* 2009; **31**: 885–896.
  - 38 Iversen, A. K., Stewart-Jones, G., Learn, G. H., Christie, N., Sylvester-Hviid, C., Armitage, A. E., Kaul, R. et al., Conflicting selective forces affect T cell receptor contacts in an immunodominant human immunodeficiency virus epitope. *Nat. Immunol.* 2006; **7**: 179–189.
  - 39 Bachmann, M. F., Ohteki, T., Faienza, K. M., Zakarian, A., Kagi, D., Speiser, D. E. and Ohashi, P. S., Altered peptide ligands trigger perforin rather than Fas-dependent cell lysis. *J. Immunol.* 1997; **159**: 4165–4170.
  - 40 Bachmann, M. F., Oxenius, A., Speiser, D. E., Mariathasan, S., Hengartner, H., Zinkernagel, R. M. and Ohashi, P. S., Peptide-induced T cell receptor down-regulation on naive T cells predicts agonist/partial agonist properties and strictly correlates with T cell activation. *Eur. J. Immunol.* 1997; **27**: 2195–2203.
  - 41 Bachmann, M. F., Speiser, D. E., Zakarian, A. and Ohashi, P. S., Inhibition of TCR triggering by a spectrum of altered peptide ligands suggests the mechanism for TCR antagonism. *Eur. J. Immunol.* 1998; **28**: 3110–3119.
  - 42 Martin, S., Kohler, H., Weltzien, H. U. and Leipner, C., Selective activation of CD8 T cell effector functions by epitope variants of lymphocytic choriomeningitis virus glycoprotein. *J. Immunol.* 1996; **157**: 2358–2365.

- 43 Achour, A., Michaelsson, J., Harris, R. A., Ljunggren, H. G., Karre, K., Schneider, G. and Sandalova, T., Structural basis of the differential stability and receptor specificity of H-2Db in complex with murine versus human beta2-microglobulin. *J. Mol. Biol.* 2006. **356**: 382–396.
- 44 Achour, A., Michaelsson, J., Harris, R. A., Odeberg, J., Grufman, P., Sandberg, J. K., Levitsky, V. et al., A structural basis for LCMV immune evasion: subversion of H-2D(b) and H-2K(b) presentation of gp33 revealed by comparative crystal structure. Analyses. *Immunity* 2002. **17**: 757–768.
- 45 Tissot, A. C., Ciatto, C., Mittl, P. R., Grutter, M. G. and Pluckthun, A., Viral escape at the molecular level explained by quantitative T-cell receptor/peptide/MHC interactions and the crystal structure of a peptide/MHC complex. *J. Mol. Biol.* 2000. **302**: 873–885.
- 46 Wang, B., Sharma, A., Maile, R., Saad, M., Collins, E. J. and Frelinger, J. A., Peptidic termini play a significant role in TCR recognition. *J. Immunol.* 2002. **169**: 3137–3145.
- 47 Pircher, H., Moskophidis, D., Rohrer, U., Burki, K., Hengartner, H. and Zinkernagel, R. M., Viral escape by selection of cytotoxic T cell-resistant virus variants in vivo. *Nature* 1990. **346**: 629–633.
- 48 Velloso, L. M., Michaelsson, J., Ljunggren, H. G., Schneider, G. and Achour, A., Determination of structural principles underlying three different modes of lymphocytic choriomeningitis virus escape from CTL recognition. *J. Immunol.* 2004. **172**: 5504–5511.
- 49 Tissot, A. C., Pecorari, F. and Pluckthun, A., Characterizing the functionality of recombinant T-cell receptors in vitro: a pMHC tetramer based approach. *J. Immunol. Methods* 2000. **236**: 147–165.
- 50 Holmberg, K., Mariathasan, S., Ohteki, T., Ohashi, P. S. and Gascoigne, N. R., TCR binding kinetics measured with MHC class I tetramers reveal a positive selecting peptide with relatively high affinity for TCR. *J. Immunol.* 2003. **171**: 2427–2434.
- 51 van Stipdonk, M. J., Badia-Martinez, D., Sluijter, M., Offringa, R., van Hall, T. and Achour, A., Design of agonistic altered peptides for the robust induction of CTL directed towards H-2Db in complex with the melanoma-associated epitope gp100. *Cancer Res.* 2009. **69**: 7784–7792.
- 52 Chen, J. L., Stewart-Jones, G., Bossi, G., Lissin, N. M., Wooldridge, L., Choi, E. M., Held, G. et al., Structural and kinetic basis for heightened immunogenicity of T cell vaccines. *J. Exp. Med.* 2005. **201**: 1243–1255.
- 53 al-Ramadi, B. K., Jelonek, M. T., Boyd, L. F., Margulies, D. H. and Bothwell, A. L., Lack of strict correlation of functional sensitization with the apparent affinity of MHC/peptide complexes for the TCR. *J. Immunol.* 1995. **155**: 662–673.
- 54 Kersh, G. J., Kersh, E. N., Fremont, D. H. and Allen, P. M., High- and low-potency ligands with similar affinities for the TCR: the importance of kinetics in TCR signaling. *Immunity* 1998. **9**: 817–826.
- 55 Pinilla-Ibarz, J., May, R. J., Korontsvit, T., Gomez, M., Kappel, B., Zakhaleva, V., Zhang, R. H. et al., Improved human T-cell responses against synthetic HLA-0201 analog peptides derived from the WT1 oncogene. *Leukemia* 2006. **20**: 2025–2033.
- 56 Hogquist, K. A., Jameson, S. C., Heath, W. R., Howard, J. L., Bevan, M. J. and Carbone, F. R., T cell receptor antagonist peptides induce positive selection. *Cell* 1994. **76**: 17–27.
- 57 Colbert, R. A., Rowland-Jones, S. L., McMichael, A. J. and Frelinger, J. A., Differences in peptide presentation between B27 subtypes: the importance of the P1 side chain in maintaining high affinity peptide binding to B\*2703. *Immunity* 1994. **1**: 121–130.
- 58 Scott, D. R., Borbulevych, O. Y., Piepenbrink, K. H., Corcelli, S. A. and Baker, B. M., Disparate degrees of hypervariable loop flexibility control T-cell receptor cross-reactivity, specificity, and binding mechanism. *J. Mol. Biol.* 2011. **414**: 385–400.
- 59 Jones, L. L., Colf, L. A., Stone, J. D., Garcia, K. C. and Kranz, D. M., Distinct CDR3 conformations in TCRs determine the level of cross-reactivity for diverse antigens, but not the docking orientation. *J. Immunol.* 2008. **181**: 6255–6264.
- 60 Reiser, J. B., Darnault, C., Guimezanes, A., Gregoire, C., Mosser, T., Schmitt-Verhulst, A. M., Fontecilla-Camps, J. C. et al., Crystal structure of a T cell receptor bound to an allogeneic MHC molecule. *Nat. Immunol.* 2000. **1**: 291–297.
- 61 Anikeeva, N., Lebedeva, T., Krosgaard, M., Tetin, S. Y., Martinez-Hackert, E., Kalams, S. A., Davis, M. M. et al., Distinct molecular mechanisms account for the specificity of two different T-cell receptors. *Biochemistry* 2003. **42**: 4709–4716.
- 62 Huseby, E. S., Crawford, F., White, J., Marrack, P. and Kappler, J. W., Interface-disrupting amino acids establish specificity between T cell receptors and complexes of major histocompatibility complex and peptide. *Nat. Immunol.* 2006. **7**: 1191–1199.
- 63 Achour, A., Harris, R. A., Persson, K., Sundback, J., Sentman, C. L., Schneider, G., Lindqvist, Y. et al., Murine class I major histocompatibility complex H-2D $\delta$ : expression, refolding and crystallization. *Acta Crystallogr. D Biol. Crystallogr.* 1999. **55**: 260–262.
- 64 Sandalova, T., Michaelsson, J., Harris, R. A., Ljunggren, H. G., Karre, K., Schneider, G. and Achour, A., Expression, refolding and crystallization of murine MHC class I H-2D $\delta$  in complex with human beta2-microglobulin. *Acta Crystallogr. Sect. F Struct. Biol. Cryst. Commun.* 2005. **61**: 1090–1093.
- 65 Sandalova, T., Michaelsson, J., Harris, R. A., Odeberg, J., Schneider, G., Karre, K. and Achour, A., A structural basis for CD8+ T cell-dependent recognition of non-homologous peptide ligands: implications for molecular mimicry in autoreactivity. *J. Biol. Chem.* 2005. **280**: 27069–27075.
- 66 Battye, T. G., Kontogiannis, L., Johnson, O., Powell, H. R. and Leslie, A. G., iMOSFLM: a new graphical interface for diffraction-image processing with MOSFLM. *Acta Crystallogr. D Biol. Crystallogr.* 2011. **67**: 271–281.
- 67 Evans, P., Scaling and assessment of data quality. *Acta Crystallogr. D Biol. Crystallogr.* 2006. **62**: 72–82.
- 68 McCoy, A. J., Grosse-Kunstleve, R. W., Adams, P. D., Winn, M. D., Storoni, L. C. and Read, R. J., Phaser crystallographic software. *J. Appl. Crystallogr.* 2007. **40**: 658–674.
- 69 Murshudov, G. N., Vagin, A. A. and Dodson, E. J., Refinement of macromolecular structures by the maximum-likelihood method. *Acta Crystallogr. D Biol. Crystallogr.* 1997. **53**: 240–255.
- 70 Emsley, P., Lohkamp, B., Scott, W. G. and Cowtan, K., Features and development of Coot. *Acta Crystallogr. D Biol. Crystallogr.* 2010. **66**: 486–501.

**Abbreviations:** APL: altered peptide ligands · CD: circular dichroism ·  $\Delta G$ : change in free energy ·  $\Delta H$ : change in enthalpy · pMHC: MHC/peptide complex ·  $\Delta S$ : change in entropy · SPR: surface plasmon resonance

**Full correspondence:** Dr. Adnane Achour, Center for Infectious Medicine, Department of Medicine, F59, Karolinska University Hospital Huddinge, Karolinska Institutet, S-141 86 Stockholm, Sweden  
Fax: +46-8-30-42-76  
e-mail: adnane.achour@ki.se

Received: 5/4/2012  
Revised: 18/6/2012  
Accepted: 23/7/2012  
Accepted article online: 26/7/2012

# European Journal of Immunology

## Supporting Information

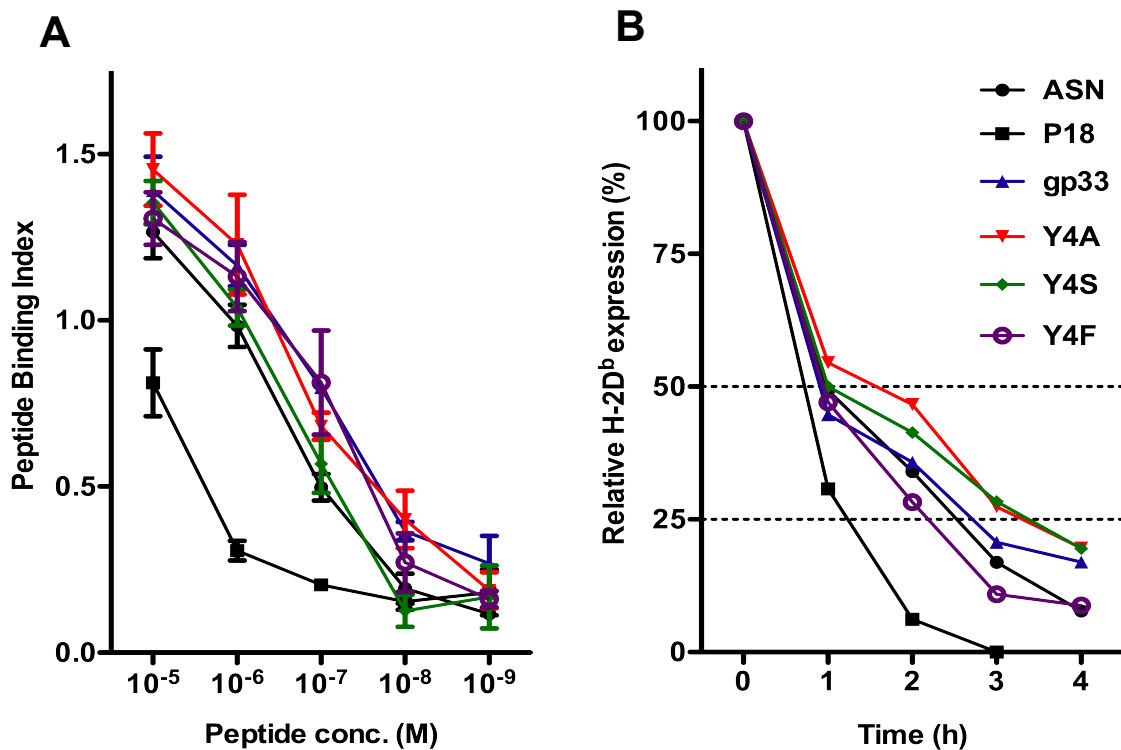
for

**DOI 10.1002/eji.201242588**

Eva B. Allerbring, Adil D. Duru, Hannes Uchtenhagen, Chaithanya Madhurantakam,  
Markus B. Tomek, Sebastian Grimm, Pooja A. Mazumdar, Rosmarie Friemann,  
Michael Uhlin, Tatyana Sandalova, Per-Åke Nygren and Adnane Achour

**Unexpected T-cell recognition of an altered peptide ligand is driven by reversed  
thermodynamics**

# Supplementary Figure 1



## A. The four peptides display similar binding affinity to H-2D<sup>b</sup>

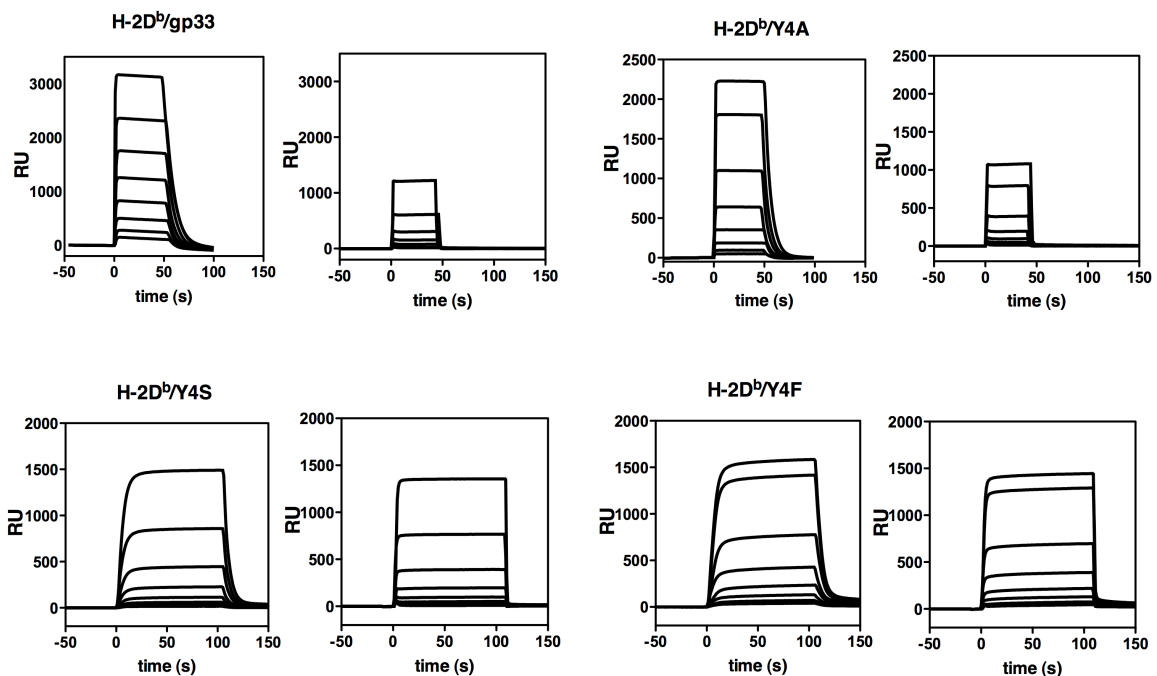
Cell surface expression of H-2D<sup>b</sup> following stabilization with wild type and gp33 APLs was tested on T2-D<sup>b</sup> cells incubated at 26°C over night at different peptide concentrations. The mean fluorescence intensity (MFI) was measured for each peptide concentration (data is a mean of three independent experiments +/- SEM). The relative peptide binding affinity was calculated using the equation  $(\text{MFI}(\text{peptide}) - \text{MFI}(\text{no peptide}) / \text{MFI}(\text{no peptide}))$ . P18 is the HIV-derived H-2D<sup>d</sup>-restricted epitope RGPGRAFVTI. ASN is the Influenza-derived H-2D<sup>b</sup>-restricted peptide ASNENMETM.

## B. The four peptides display equivalent capacity to stabilize H-2D<sup>b</sup> expression on the surface of TAP-deficient T2-D<sup>b</sup> cells

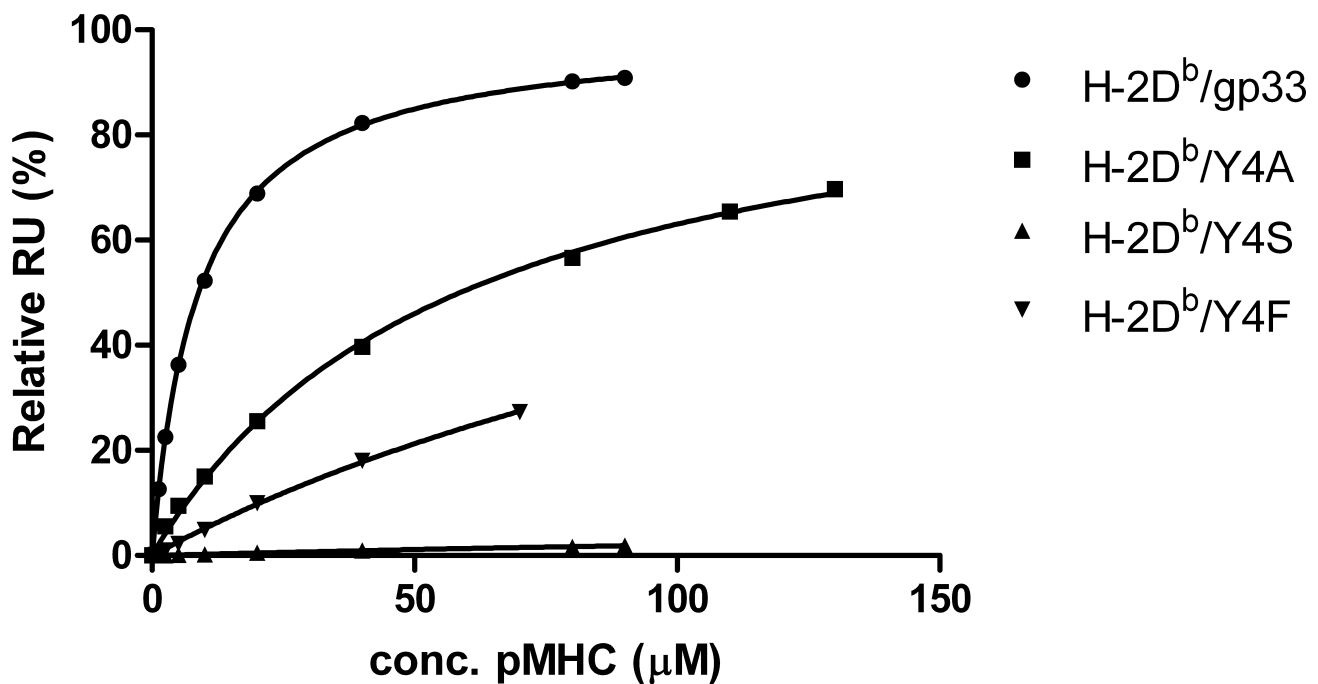
Cells were incubated with  $10^{-6}$  M of each peptide at 26°C for 12 hours in 5% CO<sub>2</sub>. Cells were collected at the time points 1, 2, 3 and 4 hours. The mean fluorescence intensity (MFI) observed for each time point was normalized as in the peptide binding affinity assays described above. One representative experiment out of three independent experiments is presented in the figure.

## Supplementary Figure 2

**A**



**B**



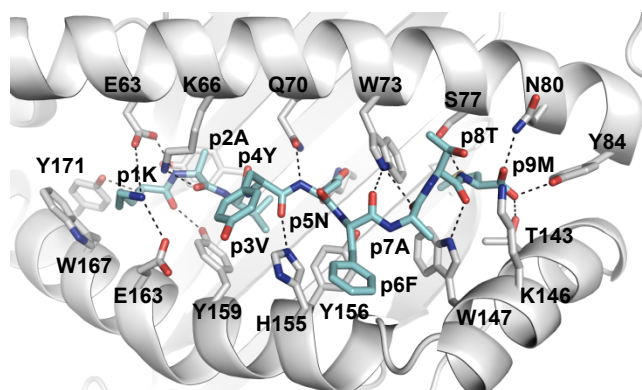
## **Binding affinity isotherms of P14 to the four H-2D<sup>b</sup> complexes correlates with the functional hierarchy**

**A.** BIACore sensorgrams for binding of each H-2D<sup>b</sup>/peptide complex to immobilized P14 TCR. Binding curves for each pMHC are displayed in the left panel while background responses from the reference surface in control flow cell are displayed in the right panel. The concentration series used is indicated within the left panel for each pMHC. All data were plotted with the injection point at 0 s. **B.** Equilibrium binding response of each pMHC to P14 as a function of pMHC concentration. Solid lines represent non-linear square fit to a one-site specific binding.  $K_D$ -values were calculated from steady state fitting of the curves, following subtraction of reference responses.  $K_D$ -values for binding of P14 to H-2D<sup>b</sup>/gp33 and H-2D<sup>b</sup>/Y4A were 8.6 and 58.6  $\mu$ M, respectively. P14 did not bind to H-2D<sup>b</sup>/Y4S and H-2D<sup>b</sup>/Y4F.

# Supplementary Figure 3

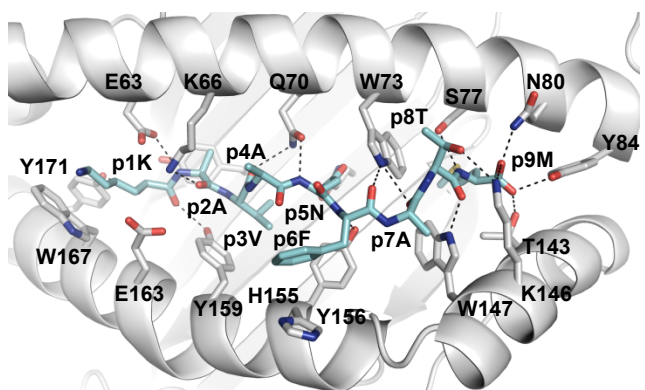
**A**

H-2D<sup>b</sup>/gp33



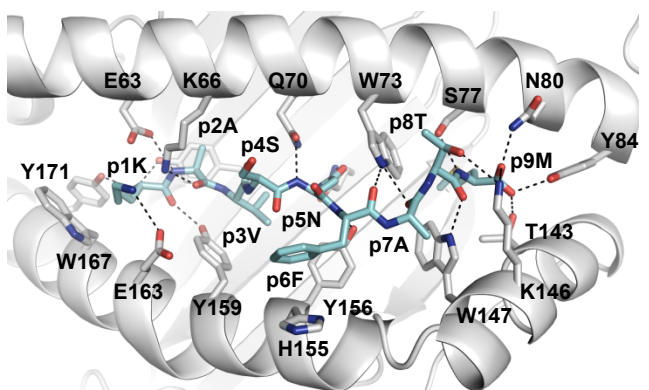
**B**

H-2D<sup>b</sup>/Y4A



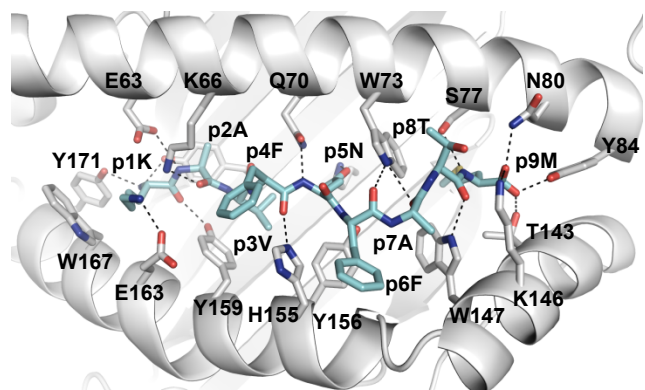
**C**

H-2D<sup>b</sup>/Y4S



**D**

H-2D<sup>b</sup>/Y4F



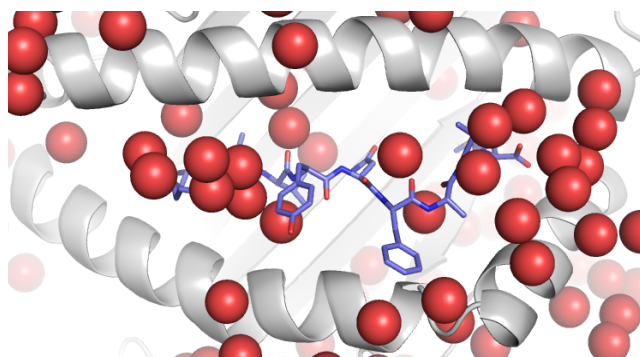
**The total amount of hydrogen bond interactions formed between H-2Db and the four peptides is equivalent.**

A schematic view of the peptide-binding cleft of H-2Db presenting the four peptides, displayed in grey. Peptides are colored light blue. Oxygen and nitrogen atoms are red and blue, respectively. All peptide residues are indicated with p. The main TCR-interaction peptide position 4 is indicated in red. The side chains of all H-2Db residues that contact each peptide are indicated. Each hydrogen bond interaction formed between H-2Db and each peptide are indicated by dotted lines. A. H-2D<sup>b</sup>/gp33, B. H-2D<sup>b</sup>/Y4A, C. H-2D<sup>b</sup>/Y4S, D. H-2D<sup>b</sup>/Y4F.

# Supplementary Figure 4

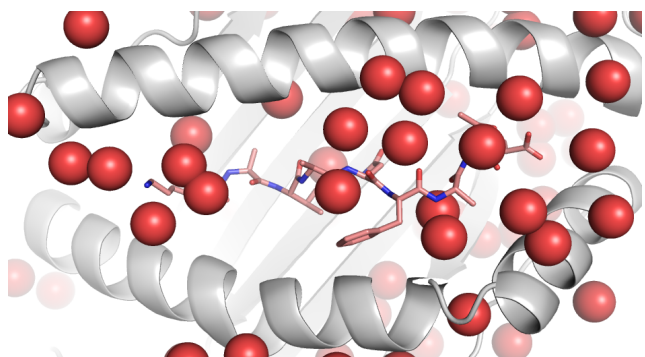
A

H-2D<sup>b</sup>/gp33



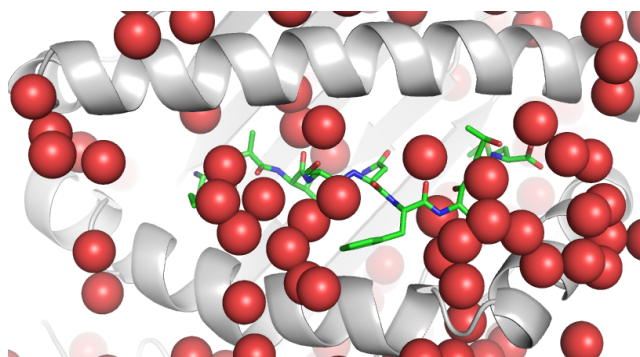
B

H-2D<sup>b</sup>/Y4A



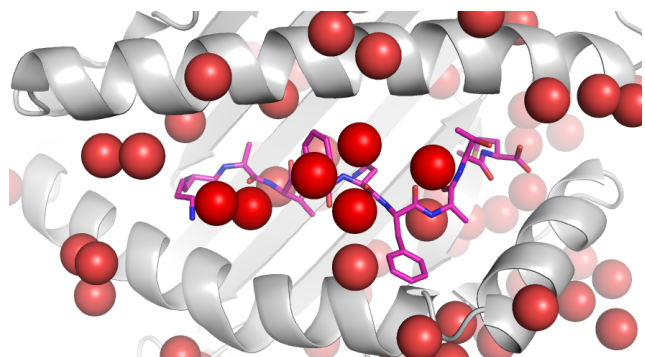
C

H-2D<sup>b</sup>/Y4S



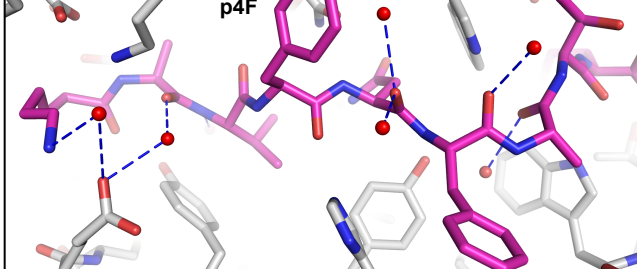
D

H-2D<sup>b</sup>/Y4F

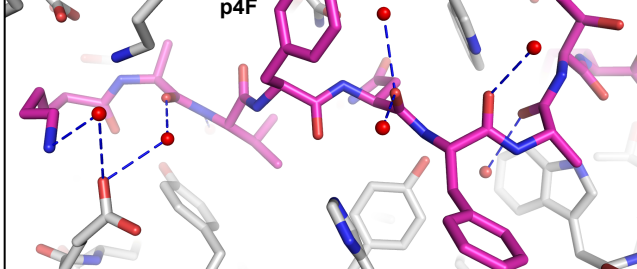


E

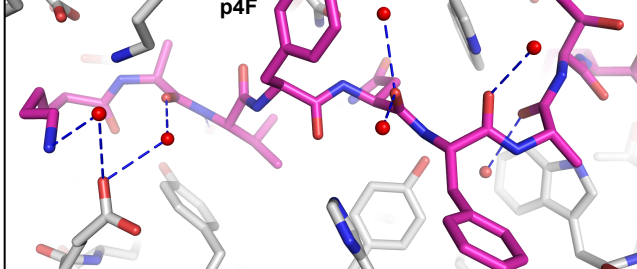
p4Y



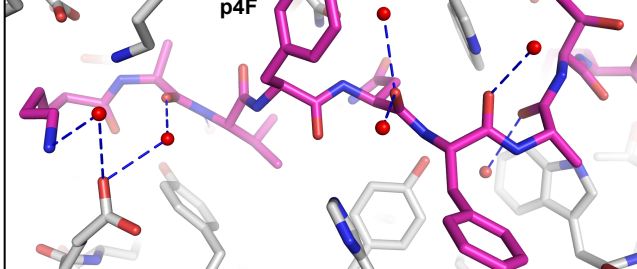
p4A



p4S



p4F



**Structural analysis revealed that although the amount of water molecules present within the binding cleft of the four pMHCs is similar, water molecules are more coordinated in H-2D<sup>b</sup>/Y4S when compared to the other three pMHCs**

All water molecules, represented as red spheres, localized within or close to the peptide-binding cleft are displayed for H-2D<sup>b</sup> in complex with A. gp33, B. Y4A, C. Y4S and D. Y4F in the upper panels. The peptides are presented as sticks, and the MHC heavy chains as cartoons. The lower panels shows a more detailed view of the water coordination around the peptides, indicated with dashed lines in the figure. The main TCR interacting position 4 is indicated. Both peptides and MHC side chains are represented as sticks. Water molecules involved in polar contacts with more than one molecule within a radius of 3.2 Å are defined as coordinated, and thus more strongly retained to the TCR-binding interface of the pMHC.